Constraints on Spin-Dependent Short-Range Interaction between Nucleons

K. Tullney,[1,*] F. Allmendinger,[2] M. Burghoff,[3] W. Heil,[1] S. Karpuk,[1] W. Kilian,[3] S. Knappe-Grüneberg,[3] W. Müller,[3] U. Schmidt,[2] A. Schnabel,[3] F. Seifert,[3] Yu. Sobolev,[1,†] and L. Trahms[3]

[1] *Institut für Physik, Johannes Gutenberg-Universität, 55099 Mainz, Germany*
[2] *Physikalisches Institut, Universität Heidelberg, 69120 Heidelberg, Germany*
[3] *Physikalisch-Technische Bundesanstalt Berlin, 10587 Berlin, Germany*

(Dated: March 27, 2013)

We report on the search for a new spin-dependent P- and T-violating interaction between nucleons mediated by light, pseudoscalar bosons such as the axion which was invented to solve the strong CP problem. Our experimental approach is to use an ultra-sensitive low-field magnetometer based on the detection of free precession of co-located ^{3}He and ^{129}Xe nuclear spins using SQUIDs as low-noise magnetic flux detectors. In the presence of an unpolarized mass the precession frequency shift was measured to determine the coupling of pseudoscalar particles to the spin of the bound neutron. For the force range from $3{\cdot}10^{-4}$ m - 10^{-1} m, corresponding to the preferred mass range between 2 μeV and 500 μeV for the axion or axion-like particles, we improved the upper bounds on the products of scalar and pseudoscalar couplings ($g_s g_p$) by up to 4 orders of magnitude.

PACS numbers: 06.30.Ft, 07.55.Ge, 11.30.Cp, 11.30.Er, 04.80.Cc, 32.30.Dx, 82.56.Na

Axions are light, pseudoscalar particles that arise in theories in which the Peccei-Quinn $U(1)$ symmetry has been introduced to solve the strong CP problem [1]. They could have been produced in early stages of the Universe being attractive candidates to the cold dark matter that could compose up to $\sim$1/3 of the ingredients of the Universe [2]. Several constraints from astrophysics, cosmology, and laboratory experiments have been applied in order to prove or rule out the existence of the axion, i.e., constrain the axions mass m_a and/or its couplings. The mass range, in which axions are still likely to exist, could thus be narrowed down to a window reaching from μeV [3] up to some meV [4] (axion window).

Most axion searches look for the conversion of a galactic [5], solar [6], or laboratory [7] origin axion into a photon in the presence of a static magnetic field. However, any axion or axion-like particle that couples with both scalar and pseudoscalar vertices to fundamental fermions would also mediate a parity and time-reversal symmetry-violating force between a fermion f and the spin of another fermion f_σ, which is parameterized by a Yukawa-type potential with range λ and a monopole-dipole coupling given by [8]:

$$V_{\rm sp}(\vec{r}) = \frac{\hbar^2 g_s^f g_p^{f_\sigma}}{8\pi m_{f_\sigma}} (\vec{\sigma}\cdot\hat{r}) \left(\frac{1}{\lambda r} + \frac{1}{r^2}\right) e^{-r/\lambda} \qquad (1)$$

$\vec{\sigma}$ is the spin vector and λ is the range of the Yukawa-force with $\lambda = \hbar/(m_a c)$. Thus, the entire axion window can be probed by searching for spin-dependent short-range forces in the range between 20 μm and 0.2 m. g_s^f and $g_p^{f_\sigma}$ are dimensionless scalar and pseudoscalar coupling constants which in our case correspond to the scalar coupling of an axion-like particle to a nucleon ($g_s^f = g_s^N$) and its pseudoscalar coupling to a polarized bound neutron ($g_p^{f_\sigma} = g_p^n$). $\hat{r}$ is the unit distance vector from the bound neutron to the nucleon. The potential given by Eq. 1 effectively acts near the surface of a massive unpolarized sample as a pseudomagnetic field and gives rise to a shift $\Delta\nu_{\rm sp} = 2{\cdot}V_\Sigma/h$, e.g., in the precession frequency of nuclear spin-polarized gases (^{3}He and ^{129}Xe), which according to the Schmidt model [9] can be regarded as an effective probe of spin-polarized bound neutrons. The potential V_Σ is obtained by integration of $V_{\rm sp}(r)$ from Eq. 1 over the volume of the massive unpolarized sample averaged over the volume of the polarized spin-sample. Based on the analytical derivation of $V_{\Sigma,\infty}$ for disc-shaped spin- and matter samples with respective thicknesses D and d [10], we can derive the following expression for V_Σ given by

$$V_\Sigma = V_{\Sigma,\infty}\cdot\eta(\lambda) = 2\pi N\kappa\frac{\lambda^2}{D}\cdot e^{-\Delta x/\lambda}\times \left(1-e^{-D/\lambda}\right)\cdot\left(1-e^{-d/\lambda}\right)\cdot\eta(\lambda)\ . \qquad (2)$$

$\eta(\lambda)$ takes account for the finite size in transverse direction of our cylindrical samples and Δx represents the finite gap between them. Furthermore, $\kappa = \hbar^2 g_s^N g_p^n/(8\pi\cdot m_n)$ and N is the nucleon number density of the unpolarized matter sample. $\eta(\lambda)$[1] is determined numerically for our cylindrically shaped spin- and matter samples at "**c**lose"-position (see Fig. 1).

Our experimental approach to search for non-magnetic, spin-dependent interactions is to use an ultra-sensitive low-field comagnetometer based on detection of free spin precession of gaseous, nuclear polarized samples [11]. The Larmor frequencies of helium and xenon in a guiding magnetic field B are given by $\omega_{\rm L,He(Xe)} = \gamma_{\rm He(Xe)}\cdot B$,

* Corresponding author: tullnek@uni-mainz.de
† on leave from: PNPI, St.Petersburg, Russia

[1] $\eta(\lambda)$ can be expressed reasonably well by the fit function $\eta_{\rm fit}(\lambda) = (1+27.8\cdot\lambda^{1.31})/(1+234\cdot\lambda^{1.31})$.

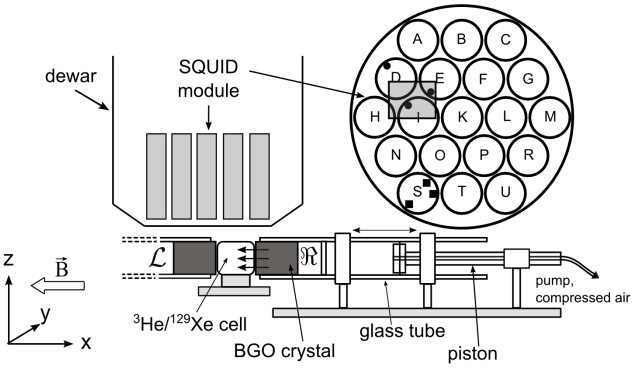

FIG. 1. Sketch of experimental setup. The dewar houses a total of 304 low-T_c DC-SQUID magnetometers which are divided up into 19 identical modules. The lower plane SQUIDs in module D, E, and I marked as (•) are used to detect the ^{3}He/^{129}Xe free spin precession. The center of the cylindrical spin sample cell ($D = 60$ mm, $\oslash_D = 58$ mm) has an average distance of $\bar{z} = 66$ mm to the sensors. The cells relative position in (x,y)-plane projection is indicated by the grey square. SQUIDs in module S marked as (■) are used for the gradiometric sensor arrangements. The unpolarized mass (cylindrical BGO crystal: $d = 70$ mm, $\oslash_d = 60$ mm) can be moved along the x-axis (B-field axis) to "close" ($\Delta x_c = 2.2$ mm) and "distant" ($\Delta x_d = 170$ mm) position and vice versa (see text). This is accomplished by a piston driven glass tube with the BGO fixed at its cell-facing side. The two arrangements left ($\mathcal{L}$) and right ($\Re$) are used.

with $\gamma_{\mathrm{He(Xe)}}$ being the gyromagnetic ratios of the respective gas species [12, 13] with $\gamma_{\mathrm{He}}/\gamma_{\mathrm{Xe}} = 2.75408159(20)$. The influence of the ambient magnetic field and its temporal fluctuations cancels in the difference of measured Larmor frequencies of the co-located spin samples

$$\Delta\omega = \omega_{\mathrm{He}} - \frac{\gamma_{\mathrm{He}}}{\gamma_{\mathrm{Xe}}} \cdot \omega_{\mathrm{Xe}} \ . \tag{3}$$

On a closer look, a resulting constant frequency shift $\Delta\omega_{\mathrm{lin}}$, e.g., due to Earth's rotation, is not compensated by co-magnetometry. That is discussed in [14], together with frequency shifts due to the generalized Ramsey-Bloch-Siegert shift which are directly proportional to the particular net magnetization $A_{\mathrm{He(Xe)}} \cdot e^{-t/T^*_{2,\mathrm{He(Xe)}}}$ and which will show up in the weighted frequency difference $\Delta\omega(t)$, too:

$$\Delta\omega(t) = \Delta\omega_{\mathrm{lin}} + \epsilon_{\mathrm{He}} \cdot A_{\mathrm{He}} \cdot e^{-\frac{t}{T^*_{2,\mathrm{He}}}} + \epsilon_{\mathrm{Xe}} \cdot A_{\mathrm{Xe}} \cdot e^{-\frac{t}{T^*_{2,\mathrm{Xe}}}} . \tag{4}$$

Accordingly, its equivalent, the weighted phase difference $\Delta\Phi(t) = \Phi_{\mathrm{He}}(t) - \frac{\gamma_{\mathrm{He}}}{\gamma_{\mathrm{Xe}}} \cdot \Phi_{\mathrm{Xe}}(t)$, is sensitive to a phase drift given by

$$\Delta\Phi(t) = \Phi_0 + \Delta\omega_{\mathrm{lin}} \cdot t - \epsilon_{\mathrm{He}} \cdot T^*_{2,\mathrm{He}} \cdot A_{\mathrm{He}} \cdot e^{-\frac{t}{T^*_{2,\mathrm{He}}}} - \epsilon_{\mathrm{Xe}} \cdot T^*_{2,\mathrm{Xe}} \cdot A_{\mathrm{Xe}} \cdot e^{-\frac{t}{T^*_{2,\mathrm{Xe}}}} \ . \tag{5}$$

Due to the knowledge of these side effects, any anomalous frequency shifts generated by non-magnetic spin interactions, such as the quested short range interaction, can be analyzed by looking at $\Delta\omega(t)$ and $\Delta\Phi(t)$, respectively. A sudden frequency change $\Delta\omega_{\mathrm{sp}}$ stemming from the pseudoscalar Yukawa potential $V_{\mathrm{sp}}(r)$ would occur at an instant $t = t_0$, e.g., by moving a massive matter sample close to the precessing nuclei. This would lead to an additional linear phase drift $\Delta\omega_{\mathrm{sp}} \cdot t$ in Eq. 5 for $t > t_0$. For further analysis, it is useful to develop Eq. 5 in a polynomial of 5th order[2] around t_0. The weighted phase difference $\Delta\Phi(t)$ can then be described by

$$\Delta\Phi_{\mathrm{fit}}(t') = a + b(t') \cdot t' + c \cdot t'^2 + d \cdot t'^3 + e \cdot t'^4 + f \cdot t'^5, \tag{6}$$

with $t' = t - t_0$. The coefficient of the linear term now reads

$$b(t') = \Delta\omega_{\mathrm{lin}} + \Delta\omega_{\mathrm{sp}}(t') - \epsilon_{\mathrm{He}} \cdot A_{\mathrm{He}} - \epsilon_{\mathrm{Xe}} \cdot A_{\mathrm{Xe}}. \tag{7}$$

Note that $\Delta\omega_{\mathrm{sp}}(t') = 2\pi \cdot \Delta\nu^w_{\mathrm{sp}} \cdot \Theta(\pm t')$ [3] is the only time dependent term in Eq. 7, so that a change of $b(t')$ at $t = t_0$ would directly indicate the existence of the short range interaction. This statement, the fit-function of Eq. 6 is based on, is valid as long as susceptibility related artefacts of the BGO crystal at its respective positions do not lead to different relaxation times T^*_2. With our special choice of $t' = t - t_0$, the linear coefficient of the Taylor expansion does not dependent on T^*_2 and thus is insensitive to possible changes in T^*_2. The impact of the T^*_2-dependence of higher order terms on $b(t')$ is discussed in detail in section *systematic uncertainties*.

The experiments were performed inside the magnetically shielded room BMSR-2 at the Physikalisch-Technische Bundesanstalt Berlin (PTB)[15]. A homogeneous guiding magnetic field of about 350 nT was provided inside the shielded room by means of a square coil pair (B_x-coils) of edge length 1800 mm. A second square coil pair (B_y-coils) arranged perpendicular to the B_x-coils was used to manipulate the sample spins, e.g., $\pi/2$ spin flip by non-adiabatic switching [11]. The main parts of the experimental setup within BMSR-2 are shown in Fig. 1. For detection of the spin precession we used a multi-channel low-T_c DC-SQUID device which was originally designed for biomagnetic applications [16, 17]. The ^{3}He/^{129}Xe nuclear spins were polarized outside the shielding by means of optical pumping. Low-relaxation cylindrical glass cells (GE180) were filled with the polarized gases and placed directly beneath the dewar as close as possible to the SQUID sensors. The SQUID sensors detect a sinusoidal change in magnetic flux due to the spin precession of the gas atoms in the glass cell. In order to obtain a high common mode rejection ratio, three first order gradiometric sensor combinations were used in order to suppress

[2] The criterium to choose a polynomial expansion up to the 5th order was that the reduced χ^2/d.o.f. of the fit equals 1.

[3] (±) in the argument of the Heaviside step function has to be set (-) for the sequence c→d and (+) for the reverse one d→c. Furthermore, for runs j = 1, 2, 3 the BGO was moved at t_0=8700 s, otherwise at t_0=10800 s .

environmental disturbance fields like vibrational modes. Fig. 1 shows their positions with respect to each other and with respect to the ^{3}He/^{129}Xe sample cell. The system noise of the SQUID gradiometer configurations was between 3 $\mathrm{fT}/\sqrt{\mathrm{Hz}}$ and 10 $\mathrm{fT}/\sqrt{\mathrm{Hz}}$ in the range of the ^{3}He/^{129}Xe spin-precession frequencies, i.e., 4 Hz $< \nu_L <$ 12 Hz, while typical signal amplitudes reached 10 pT for helium and 3 pT for xenon at the beginning of the spin precession cycle. The optimum conditions in terms of long transverse relaxation times (T_2^*) and high signal-to-noise ratio (SNR) were met at a gas mixture with pressures of $^3\mathrm{He} : {}^{129}\mathrm{Xe} : N_2 \approx (2 : 8 : 35)$ mbar, typically. Nitrogen was added to suppress spin-rotation coupling in bound Xe-Xe van der Waals molecules [18, 19]. As unpolarized matter sample we used a cylindrical BGO crystal ($Bi_4Ge_3O_{12}$, ρ=7.13 g/cm^3). BGO has a high nucleon number density, is a non-conductive material that shows low Johnson-Nyquist noise and is said to have an unusual magnetism-related behaviour in weak constant magnetic fields ($\chi_{mag} \approx 0$ ppm) [20–22]. For systematic checks, primarely to look for magnetic susceptibility related false effects, the BGO crystal could be placed left ($\mathcal{L}$) and right ($\Re$) with respect to the ^{3}He/^{129}Xe sample cell (see Fig. 1). Since $V_{\mathrm{sp}}(\vec{r}) \propto \vec{\sigma} \cdot \hat{r}$, $\Delta\nu_{\mathrm{sp}}$ changes its sign in going from $\mathcal{L}$ to $\Re$. That has to be considered by averaging the $\mathcal{L}$ and $\Re$ results. On the other hand, $\Delta\nu_{\mathrm{sp}}$ drops out averaging $\mathcal{L}$ and $\Re$ without sign change. In case of a non-zero spin-dependent axion fermion interaction, a shift $\Delta\nu_{\mathrm{sp}}^w$ in the weighted frequency difference (Eq. 3) can be extracted from respective frequency measurements in "close" and "distant" position given by

$$\Delta\nu_{\mathrm{sp}}^w = \frac{2V_\Sigma^c}{h} \cdot \left(1 - \frac{\gamma_{\mathrm{He}}}{\gamma_{\mathrm{Xe}}}\right), \tag{8}$$

assuming $V_{\Sigma,\mathrm{He}} = V_{\Sigma,\mathrm{Xe}} = V_{\Sigma,n} \equiv V_\Sigma$ (Schmidt model) and $V_\Sigma^d \ll V_\Sigma^c$.

We performed 10 measurement runs lasting approximately 9 h each. For each measurement run after $t_0 \approx 3$h the BGO crystal was moved from "close to distant" position (c→d) or vice versa (d→c). The asymmetric timing takes account for the smaller SNR in the second measurement block due to the exponential damping (T_2^*) of the signal amplitude which was $T_{2,\mathrm{He}}^* \approx 48$ h and $T_{2,\mathrm{Xe}}^* \approx 5$ h, typically. By this measure, comparable statistics was obtained for both BGO positions.

As discussed in detail in [14], the data of each run were divided into sequential time intervals of $\tau = 3.2$ s. For each obtained sub-data set, a χ^2-minimization was performed using an appropriate fit-function to extract the phases ϕ_{He}, ϕ_{Xe} and the frequencies ω_{He}, ω_{Xe} with the corresponding errors. In a further step, the accumulated phase $\Phi_{\mathrm{He(Xe)}}(t)$ was determined for each run in order to derive the weighted phase difference $\Delta\Phi\,(t)$. Then we fitted Eq. 6 simultaneously to the data of $\Delta\Phi(t)$ determined for the three gradiometers for each measurement run. From the resulting fit parameters $\overline{a}$, $\overline{b}_{\mathrm{c}}$, $\overline{b}_{\mathrm{d}}$, $\overline{c}$, $\overline{d}$, $\overline{e}$, $\overline{f}$ and by use of Eqs. 8 and 7, the frequency shift $\overline{\Delta\nu}_{\mathrm{sp}}$ is then extracted from

$$\overline{\Delta\nu}_{\mathrm{sp}} = \frac{\bar{b}_c - \bar{b}_d}{2\pi \cdot (1 - \frac{\gamma_{\mathrm{He}}}{\gamma_{\mathrm{Xe}}})} \ . \tag{9}$$

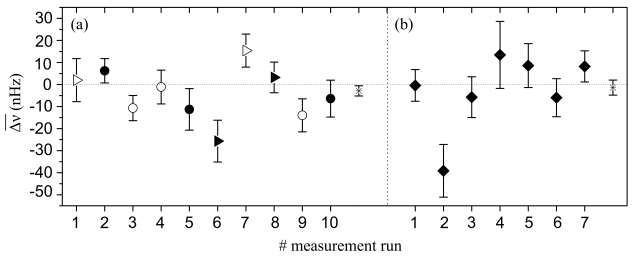

FIG. 2. (a) Extracted frequency shifts $\overline{\Delta\nu}_{\mathrm{sp}}$ (with correlated 1σ error) of the 10 measurement runs. The triangles specify the $\Re$, the circles the $\mathcal{L}$ arrangement of the BGO crystal. Full symbols indicate the c→d sequence, hollow symbols the opposite case (d→c). (b) Results $\overline{\Delta\nu}_{\mathrm{check}}$ obtained from the LV-data using the same fit-model (Eq. 6). Since no mass was moved, we expect no shift in the spin precession frequency. The rightmost symbols in both plots (stars) indicate the respective weighted means (1σ error).

For 6 runs (# : 2, 3, 4, 5, 9, 10), the BGO crystal was positioned at $\mathcal{L}$ otherwise at $\Re$. For all $\mathcal{L}$ runs, the results are multiplied by (-1): $\overline{\Delta\nu}_{\mathrm{sp}} = -\overline{\Delta\nu}_{\mathrm{sp},\mathcal{L}}$. In Fig. 2a, values $\overline{\Delta\nu}_{\mathrm{sp}}$ for the individual runs are shown together with their correlated 1σ errors[4]. Calculating the weighted mean we get $\overline{\overline{\Delta\nu}}_{\mathrm{sp}} = (-2.9 \pm 2.3)$ nHz. As consistency check, we re-analysed our 2009 data, where we looked for a possible Lorentz-violating (LV) sidereal frequency modulation [14]. Since no mass was moved, $\bar{b}_c = \bar{b}_d$ should hold, using the fit-function of Eq. 6 and a hypothetical time $t_0 = 10800$ s. Fig. 2b shows the results $\overline{\Delta\nu}_{\mathrm{check}}$ for all 7 measurement runs, again with their correlated 1σ errors. The weighted mean of the LV-data gives $\overline{\overline{\Delta\nu}}_{\mathrm{check}} = (-1.4 \pm 3.4)$ nHz. The χ^2/d.o.f of the data to their respective weighted means ($\overline{\overline{\Delta\nu}}_{\mathrm{sp}}$, $\overline{\overline{\Delta\nu}}_{\mathrm{check}}$) gives 2.29 and 2.38, indicating that the errors on the measured frequency shifts (Fig. 2) are somewhat underestimated. In order to take this into account, the errors were scaled to obtain a χ^2/d.o.f of one, as recommended, e.g., by [23, 24].

At the 95% C.L., our results for the measured frequency shifts are:

$$\overline{\overline{\Delta\nu}}_{\mathrm{sp}} = (-2.9 \pm 6.9)\ \mathrm{nHz} \tag{10}$$

$$\overline{\overline{\Delta\nu}}_{\mathrm{check}} = (-1.4 \pm 10.5)\ \mathrm{nHz} \tag{11}$$

[4] The correlated errors are calculated as square root of the diagonal elements of the covariance matrix of the least χ^2 fit-model of Eq. 6 with the proper statistical weights. The uncorrelated errors are about a factor of 30 smaller and not included in the error bars shown in Fig. 2.

indicating that i) we find no evidence for a pseudoscalar short-range interaction mediated by axion-like particles and ii) the cross check analysis of our LV-data within the error bars is also compatible with zero, as expected.

Discussion of systematic uncertainties:
The movement of the BGO-crystal can produce correlated effects that may mimic a pseudoscalar frequency shift or even compensate the effect we are looking for. Two effects caused by a non-zero magnetic susceptibilty of the BGO have to be considered.
a.) The BGO at "close" position slightly changes the magnetic field across the volume of the ^{3}He/^{129}Xe sample cell. This effect drops out to first order due to comagnetometry. To second order, however, the imperfect geometrical overlap of helium and xenon resulting from the difference in their molar masses leads to a difference (Δz) in their center of masses (c.o.m) in the gravitational field of the earth according to the barometric formula. For our cylindrical sample cell this value is $\Delta z = 1.2 \cdot 10^{-7}$ m. With $\chi_{\rm BGO} = -19$ ppm, which is the susceptibility of the BGO in the high field limit ($B > 0.1$ T) [21], a conservative estimation of the systematic effect can be calculated. Therefore the field distribution across the ^{3}He/^{129}Xe sample cell, with BGO in "close" position and $B_{\rm x} = 350$ nT, was calculated with *COMSOL Multiphysics*, a finite element analysis software. From that we derived induced magnetic field gradients in vertical direction of $|\langle \partial B/\partial z\rangle|_{ind} \leq 0.08$ pT/cm, which lead to a frequency shift of $\Delta\nu_{sys}^{\rm c.o.m.} = \Delta z \cdot |\langle \partial B/\partial z\rangle|_{ind} \cdot \gamma_{\rm He}/2\pi = 0.03$ nHz. Compared to the measured frequency shift (Eq. 10), this systematic effect is negligible.
b.) More serious is the fact that a change of the magnetic field gradient by the BGO also influences the T_2^*-times of ^{3}He and ^{129}Xe. According to [11, 25, 26], the change in T_2^* for a spherical cell of radius R can be expressed by

$$\frac{\Delta T_2^*}{(T_2^*)^2} = \frac{(T_2^*)_c - (T_2^*)_d}{(T_2^*)^2} \approx \frac{8R^4\gamma^2}{175 D^{\rm GM}} \times$$

$$\left((\langle \partial B_x/\partial x\rangle_F + \langle \partial B_x/\partial x\rangle_{ind})_c^2 - (\langle \partial B_x/\partial x\rangle_F)_d^2 \right) \ , \quad (12)$$

where $D^{\rm GM}$ is the diffusion coefficient of the gas mixture [11] with $D_{\rm He}^{\rm GM} \approx 17{\rm cm}^2/{\rm s}$ and $D_{\rm Xe}^{\rm GM} \approx 4.7{\rm cm}^2/{\rm s}$, respectively. For our cylindrically shaped cell we use here the approximation $\oslash_D/2 = D/2 \approx R = 30$ mm. The BGO as diamagnet shows its strongest influence ("close" position) along the direction of the applied B_x-field which was calculated to be $\langle \partial B_x/\partial x\rangle_{ind} = \pm 0.47$ pT/cm across the sample cell. The (+) and (-) signs indicate the two BGO arrangements $\mathcal{L}$ and $\Re$, respectively.
Knowing $\langle \partial B_x/\partial x\rangle_F$ of the guiding field inside BMSR-2, $\Delta T_2^*/(T_2^*)^2$ can be calculated, in principle. The more direct approach, however, is to extract T_2^* and thus ΔT_2^* via the exponential decay of the signal amplitudes with the BGO in "close" and "distant" position. The most accurate distinction between $(T_2^*)_c$ and $(T_2^*)_d$ was obtained through a fit to the amplitude ratio $A_{Xe}(t')/A_{He}(t')$ given by

$$f_{\rm fit}(t') = W \cdot e^{-t'/T_{\rm eff}^*} \quad (13)$$

with $T_{\rm eff}^* = T_{2,\rm He}^* \cdot T_{2,\rm Xe}^* / \left(T_{2,\rm He}^* - T_{2,\rm Xe}^*\right)$. Using

$$\frac{\Delta T_{\rm eff}^*}{(T_{\rm eff}^*)^2} = -\frac{\Delta T_{2,\rm He}^*}{\left(T_{2,\rm He}^*\right)^2} + \frac{\Delta T_{2,\rm Xe}^*}{\left(\mathrm{T}_{2,\rm Xe}^*\right)^2} \approx -0.5 \frac{\Delta T_{2,\rm He}^*}{\left(T_{2,\rm He}^*\right)^2} \quad (14)$$

(see Eq. 12), a possible T_2^*-change of $\left|\Delta T_{2,\rm He}^*\right| < 160$s can be inferred from this fitting procedure. From that the systematic frequency shift $\Delta\nu_{\rm sys}^{T_2^*}$ on $b(t')$ due to higher order terms of Eq. 6, which has the same signature as the pseudoscalar phase shift, can be estimated to be[5]

$$\left|\Delta\nu_{\rm sys}^{T_2^*}\right| \leq \left| \frac{-2 \cdot \left(E_{\rm He} \cdot \frac{\Delta T_{2,\rm He}^*}{(T_{2,\rm He}^*)^3} + E_{\rm Xe} \cdot \frac{\Delta T_{2,\rm Xe}^*}{(T_{2,\rm Xe}^*)^3} \right) \cdot \langle t'\rangle_{t'}}{2\pi(1 - \gamma_{\rm He}/\gamma_{\rm Xe})} \right| , \quad (15)$$

with $E_{\rm He(Xe)} = \epsilon_{\rm He(Xe)} \cdot A_{\rm He(Xe)} \cdot T_{2,\rm He(Xe)}^*$. Here we used Eq. 9, replacing $\bar{b}_c$ and $\bar{b}_d$ by the temporal means $2 \cdot \bar{c}_c \cdot \langle t'\rangle_{t'}$ and $2 \cdot \bar{c}_d \cdot \langle t'\rangle_{t'}$ of the quadratic term (Eq. 6) with $\bar{c}_{c(d)} = \left\{ (E_{\rm He}/2)/(T_{2,\rm He}^*)^2 + (E_{\rm Xe}/2)/(T_{2,\rm Xe}^*)^2 \right\}_{c(d)}$.
From the fit function (Eq. 5) applied to the data, values for the respective $E_{\rm He(Xe)}$ amplitudes can be extracted, i.e., $-25 \leq E_{\rm He} \leq -4$ and $E_{\rm Xe} \approx 0.2$. Finally, taking $\langle t'\rangle_{t'} \approx t_0/2$ and by use of Eq. 14 we get

$$\left|\Delta\nu_{\rm sys}^{T_2^*}\right| \leq \left| \frac{-\frac{\Delta T_{2,\rm He}^*}{(T_{2,\rm He}^*)^2} \cdot \left(\frac{E_{\rm He}}{T_{2,\rm He}^*} + \frac{1}{2}\frac{E_{\rm Xe}}{T_{2,\rm Xe}^*} \right) \cdot t_0}{2\pi(1 - \gamma_{\rm He}/\gamma_{\rm Xe})} \right| \approx 0.2 \ {\rm nHz} \ . \quad (16)$$

From that, a conservative estimate on the systematic error can be made with $|\Delta\nu_{\rm sys}^{T_2^*}| = \pm 0.4$ nHz (95% C.L.). That brings us to the final result

$$\overline{\overline{\Delta\nu}}_{\rm sp} = (-2.9 \pm 6.9 \pm 0.4) \ {\rm nHz} \quad (95\% \ {\rm C.L.}) \quad (17)$$

for the measured pseudoscalar frequency shift.
From the total error $\delta(\overline{\overline{\Delta\nu}}_{\rm sp}) = \pm 7.3$ nHz we can then derive exclusion bounds for $\left|g_s^N g_p^n\right|$ using Eq. 2 and $|\delta(\overline{\overline{\Delta\nu}}_{\rm sp})| \geq 2 \cdot V_\Sigma^c/h$ which are shown in Fig.3.
We have substantially improved the bounds on a spin-dependent short-range interaction between polarized (bound) neutrons and unpolarized nucleons over most of the axion window, tightening existing constrains on axion-like particles heavier than 20 μeV by up to four orders of magnitudes.
And there are clear strategies on how to improve our experimental sensitivity: i) Close contact of the spin

[5] Contributions of terms $n \geq 3$ (Eq. 6) to the systematic error can be neglected.

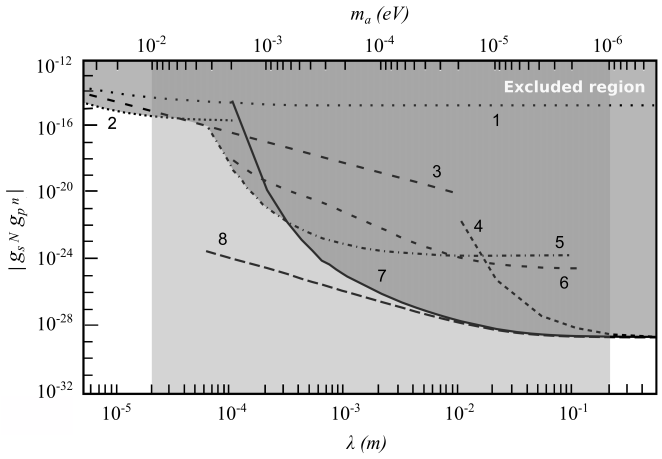

FIG. 3. The experimental 95% confidence upper limit on $\left|g_s^N g_p^n\right|$ plotted versus λ, the range of the Yukawa-force with $\lambda = \hbar/(m_a c)$. The axion window is indicated by the light grey area. (1): result of [28], (2): result of [29], (3): result of [30], (4): result of [31], (5): result of [32], (6): result of [33], (7): this experiment. See [34] for bounds on the pseudoscalar short-range force between polarized electrons and unpolarized nucleons. The expected results for Δx$\approx$ 0 mm (8) using the same data set demonstrates the gain in measurement sensitivity for $\lambda < 10^{-3}$ m by reducing the minimal gap between the polarized and unpolarized matter sample.

system with the matter sample. For $\Delta x \approx 0$ mm, our present measurement senitivity will significantly increase for $\lambda < 10^{-3}$ m (see Fig.3). ii) Moving the spin/matter sample more frequently between its set positions (c$\leftrightarrow$d and/or $\mathcal{L} \leftrightarrow \Re$). This results in a different time structure for the linear term in the fit model of Eq. 6 such that the correlated error approaches the uncorrelated one. This was demonstrated in [14], already. iii.) Magnetic susceptibility related artefacts have to be eliminated by taking zero-susceptibility matched matter samples ($\chi_{\mathrm{mag}} \approx$ 0 ppm) as it is common practice in high resolution NMR spectroscopy [27].

This work was supported by the Deutsche Forschungsgemeinschaft (DFG) under contract number BA 3605/1-1 and the research center "Elementary Forces and Mathematical Foundations" (EMG) of the university in Mainz, and by PRISMA cluster of excellence at Mainz. We are grateful to our glass blower R. Jera for preparing the low relaxation glass cells from GE180.

[1] C.D. Peccei, and H.R. Quinn, Phys. Rev. Lett., **38**, 1440 (1977)
[2] J. Jaeckel, and A. Ringwald, Annu. Rev. Nucl. Part. Sci., **60**, 405 (2010)
[3] S. Asztalos et al., Phys. Rev. D, **69**, 011101(R)) (2004)
[4] G. Raffelt, Annu. Rev. Nucl. Part. Sci., **49**, 63 (1999)
[5] S. Asztalos et al., Phys. Rev. Lett., **104**, 041301 (2009)
[6] E. Arik et al., J. Cosmol. Astropart. Phys., **02**, 008 (2009)
[7] K. Ehert et al., Phys. Rev. Lett., **689**, 149 (2010)
[8] J.E. Moody, and F. Wilczek, Phys. Rev. D, **30**, 130 (1984)
[9] Th. Schmidt, Zeitschrift für Physik A Hadrons and Nuclei, **10**6, 358 (1937)
[10] O. Zimmer, Phys. Lett. B, **38**, 685 (2010)
[11] C. Gemmel et al., Eur. Phys. Journal D, **57**, 303 (2010)
[12] M. Pfeffer and O. Lutz, J. Magn. Res. A, **108**, 106 (1994)
[13] International council for Science: Committee on Data for Science and Technology (CODATA), www.codata.org (2007)
[14] C. Gemmel et al., Phys. Rev. D, **82**, 111901 (2010)
[15] J. Bork et al., Proc. Biomag., **2000**, 970 (2000)
[16] D. Drung, Physica C, **368**, 134 (2002)
[17] M. Burghoff et al., IEEE Trans. App. Supercon., **17**, 846 (2007)
[18] B. Chann et al., Phys. Rev. Lett., **88**, 113201 (2002)
[19] B.C. Anger et al., Phys. Rev. A, **78**, 043406 (2008)
[20] E.A. Kravchenko, V.G. Orlov, and M.P. Shlykov, Russian Chemical Reviews, **75(1)**, 77-93 (2006)
[21] S. Yamamoto, K. Kuroda and M. Senda, IEEE Transactions On Nuclear Science, **50**, 1683 (2003)
[22] B. C. Grabmaier, and R. Oberschmid, Phys. Stat. Sol., **(a) 96**, 199 (1986)
[23] The Particle Data Group, Phys. Lett. B, **592**, 14 (2004)
[24] W.H. Press, S.A. Tenkolsky, W.T. Vetterling, and B.P. Flannery, *Numerical Recipes 3rd Edition: The Art of Scientific Computing.*, Cambridge University Press, New York (2007)
[25] G.D. Cates, S.R. Schaefer, and W. Happer, Phys. Rev. A, **37**, 2877 (1988)
[26] W. Kilian et al., Eur. Phys. J. D, **42**, 197 (2007)
[27] R. Ravi et al., J. Magn. Res., textbf205, 63 (2010)
[28] S. Baeler et al., Phys. Rev. D, **75**, 075006 (2007)
[29] T. Jenke et al., arXiv: 1208.3875v1 (2012)
[30] A.P. Serebrov et al., JETP Letters, **91**, 6 (2010)
[31] A.N. Youdin et al.,Phys. Rev. Lett., **77**, 2170 (1996)
[32] M. Bulatowicz et al., arXiv: 1301.5224v1 (2013)
[33] P.-H. Chu et al., Phys. Rev. D, **87**, 011105(R) (2013)
[34] S.A. Hoedel, Phys. Rev. Lett., **106**, 041801 (2011)